Digest Journal of Nanomaterials and Biostructures Vol. 7 No. 3, July - September 2012, p. 1103 - 1115

FREQUENCY AND SENSITIVITY ANALYSIS OF ATOMIC FORCE MICROSCOPE (AFM) CANTILEVER CONSIDERING COUPLED FLEXURAL-TORSIONAL VIBRATIONS

MINA MOOSAPOUR, MOHAMMAD A. HAJABASI*,
HOSSEIN EHTESHAMI
Department of Mechanical Engineering, Shahid Bahonar University of Kerman, Kerman, P.O.Box:761175-133, Iran.

Frequency analysis and modal sensitivity of an atomic force microscope (AFM) cantilever is presented in this paper. Closed-form expressions for frequency equation and sensitivity of vibration modes are derived for the tip-cantilever system as the cantilever undergoes coupled lateral-vertical bending with torsional vibration. In this work, the effects of the sample surface contact stiffness and the cantilever to tip lengths ratio on resonant frequencies and sensitivities are assessed. The results show that the resonant frequency is constant in low and high values of the normal and lateral contact stiffnesses and there is a shift of frequency in a specific value of stiffness. Also, in comparison with the values of normal contact stiffness, frequency shift, due to the tip–sample interaction, occurs in lower values of lateral contact stiffness. In the low values of contact stiffnesses, the lower-order vibration modes are more sensitive than the higher-order modes. The situation is completely reversed in very high contact stiffnesses. In addition the resonant frequencies are more sensitive to the variation of lateral contact stiffness with respect to the variation of normal contact stiffness.

(Received May 28, 2012; Accepted August 1, 2012)

Keywords: Atomic force microscope cantilever, Resonant frequency, Modal sensitivity, Contact stiffnesses

1. Introduction

The AFM was invented in 1986 by Binnig, Quate and Gerber [1]. The AFM relies on a scanning technique to produce very high resolution, 3-D images of sample surfaces. The AFM measures ultra-small forces (less than 1 nN) that exist between the AFM tip surface and a sample surface. These small forces are measured by observing the motion of a very flexible cantilever beam with an ultra-small mass [2]. The deflection of the cantilever is measured by an array of photodiodes that receives the reflected laser beam from the top surface of the cantilever. These data collection can be used to determine some important characteristics of the sample surface such as friction, visco-elasticity, surface topography and many other mechanical properties. AFMs can be used to study surfaces, whether they are electrically conductive or insulating.

The principal modes of operation for an AFM are static mode and dynamic mode. In static mode, the cantilever is dragged across the surface of the sample and the contours of the surface are calculated directly using the deflection of the cantilever. In the dynamic mode, the cantilever is externally oscillated at or close to its fundamental resonance frequency by its holder or the sample. The oscillation amplitude, phase and resonance frequency are changed by the interaction force between the tip and the surface. These changes in the vibration parameters with respect to the external reference oscillation are used to reveal information about the surface properties of

*Corresponding author: hajabasi@uk.ac.ir, hajabasi@gmail.com

samples. Compared to static AFM, dynamic AFM can provide a better signal-to-noise ratio and higher resolution in measurement of material and surface properties [3]. Three types of dynamic modes of AFM can be categorized in terms of the cantilever deflection and excitation mode. They are: contact mode, non-contact mode, and tapping mode (TM); torsional resonance (TR) mode; and lateral excitation (LE) mode. In contact mode, non-contact mode, and TM, generally the cantilever is excited by the vertical harmonic motion of its holder. In TR mode, two piezoelectric elements are attached to the cantilever holder and vibrate out-of-phase to drive the cantilever into torsional oscillation. In LE mode, the cantilever is driven by the lateral motion of the sample through tip–sample interaction [4].

In a series of works, Bhushan et al. [3-6] have developed the analytical and numerical models for dynamic simulation of AFM cantilevers at different dynamic modes with and without tip–sample interaction. Song et al [4] was developed the 3D Finite Element beam model of tip–cantilever systems for numerical simulation of free and surface-coupled dynamics of tip–cantilever system in various dynamic modes of AFM.

The imaging rate and contrast of topographic images can be influenced by the resonant frequency and modal sensitivity, respectively. Therefore, the study of the resonant frequency and the sensitivity of an AFM cantilever are significant and have been investigated by many researchers. Turner and Wiehn [7] have studied the sensitivities of the flexural and torsional modes for AFM cantilevers and derived a closed-form expression for cantilevers with constant cross sections. They have developed an approximate solution for cantilevers with other shapes using the method of Rayleigh–Ritz. They found that the shape of the cantilever can considerably affect the modal sensitivity. Chang [8] have studied the sensitivity of flexural vibration modes for the rectangular cantilever of an AFM and obtained a closed-form expression by taking into account the cantilever slope. He perceived that increase of the cantilever slope apparently decreases the sensitivity at low contact stiffness. Chang et al. [9] analyzed the interactive damping effect occurring between the cantilever tip and sample surface on the sensitivity of flexural and torsional vibration modes of AFM rectangular cantilever. They derived a closed-form expression for the frequency equation and flexural and torsional sensitivity. They observed that sensitivity of flexural and torsional of first mode decreased with increasing normal and lateral interactive damping when the normal and lateral contact stiffness was low. Hsu et al. [10] studied the flexural vibration for an AFM cantilever using the Timoshenko beam theory and presented a closed-form expression for the frequencies of vibration modes. They demonstrated that the Timoshenko beam theory is able to predict the frequencies of flexural vibration of the higher modes with higher contact stiffness. Without considering vertical bending, Lee et al. [11] investigated the influence of the contact stiffness and the cantilever to tip lengths ratio on the resonant frequency and the sensitivity of lateral vibration modes. In their study, the cantilever can vibrate in a combination of torsion and lateral bending modes. Kahrobaiyan et al. [12] studied resonant frequencies and flexural sensitivities of an AFM with assembled cantilever probe (ACP). They assessed the effects of the sample surface contact stiffness and some geometrical parameters on both flexural and torsional resonant frequencies and sensitivities.

Generally, a vibrating cantilever has four uncoupled deflection: namely vertical bending, lateral bending, torsion and extension. For a rectangular cantilever, the torsional and lateral stiffness are nearly two and the extension stiffness is four to five orders of magnitude higher than the vertical stiffness. Thus in this paper, the displacement component that is related to the extension, can be neglected.

In contact mode, non-contact mode and TM, vertical bending dominates the deflection of the cantilever, whereas in TR and LE modes the deflection of the cantilever is in fact a combination of torsion and lateral bending. These couplings between the vertical bending, lateral bending and torsion are generally ignored in the literature for the sake of simplicity. Hence, a model that can consider all the couplings is very desirable. In this paper, by considering the coupling of lateral-vertical bending with torsional vibration (flexural-torsional), the resonant frequencies and the modal sensitivities analyses are carried out using an analytical method. The flexural-torsional coupling is due to the presence of the tip–sample interaction. Effects of normal and lateral contact stiffnesses and the cantilever to tip lengths ratio on the natural frequencies and the modal sensitivities of the system will be presented.

2. Analysis

2.1. Basic equation

Fig.1 shows the schematic diagram of an AFM cantilever in contact with a sample. The deflection of the cantilever is measured by an array of photodiodes that receives the reflected laser beam from the top surface of the cantilever. In this paper, the deflection is resolved to a rotation and two displacements. $\phi(X,t)$ is the rotation angle around the X -axis, $W(X,t)$ is the vertical displacement along the Z -axis, $V(X,t)$ is the lateral displacement along the Y -axis and extension along the X -axis in comparison with the other displacement components can be neglected. We have assumed that the AFM cantilever is parallel to the sample surface and tip is located at the end of the cantilever. To analyze the cantilever response, tip–sample interaction needs to be established first. Under small deflection, the tip–sample interaction forces in normal and tangential directions are described by three linear springs K_n, K_l and K_t respectively, which act at the end of the AFM tip. Usually, it can be assumed that $K_l = K_t$ [4]. This may be because of macroscopic surface properties which are essentially the same in all tangential directions. A probe in AFM can be modeled as a three-dimensional beam with clamped–free boundary conditions and the tip is represented by a rigid bar. As shown in Fig 1, the probe has a cross section with width D, thickness h, length L and tip length H. The lateral tip–sample interaction exerts a torque and a lateral force on the cantilever, which causes the torsional and lateral bending vibration. The normal tip-sample interaction exerts a normal force on the cantilever which causes vertical bending. Longitudinal tip–sample interaction exerts a torque and a longitudinal force on the cantilever, which cause the extension and vertical bending vibration. But we assumed that the extension is neglected.

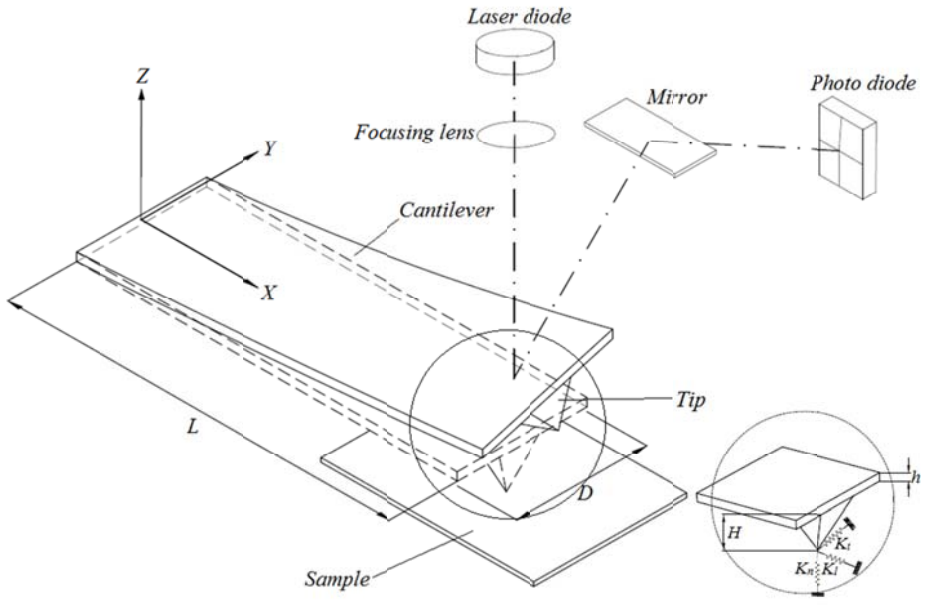

Fig. 1. Schematic diagram of an AFM tip–cantilever undergoing vertical bending, lateral bending and torsion. The tip-sample interaction forces are modeled by three linear springs K_n, K_l *and* K_t.

Therefore, the linear differential equations of motion for the vertical bending, lateral bending and torsional vibration of an Euler-Bernoulli beam are [5,13]

$$EI_y \frac{\partial^4 W(X,t)}{\partial X^4} + \rho A \frac{\partial^4 W(X,t)}{\partial t^4} = 0 \tag{1}$$

$$EI_z \frac{\partial^4 V(X,t)}{\partial X^4} + \rho A \frac{\partial^4 V(X,t)}{\partial t^4} = 0 \tag{2}$$

$$GJ \frac{\partial^2 \phi(X,t)}{\partial X^2} = \rho I_p \frac{\partial^2 \phi(X,t)}{\partial t^2} \tag{3}$$

where E and G are Young's modulus and shear modulus, ρ is the mass density, A is the cross-section area, J is the torsional constant, I_y is the moment of inertia about the Y axis, I_z is the moment of inertia about the Z axis and I_p is the polar area moment of the inertia. For a cantilever with a rectangular cross section, $A = Dh$, $I_y = Dh^3/12$, $I_z = hD^3/12$, $I_p = (Dh^3 + hD^3)/12$ and $J \approx (1/3)Dh^3(1 - 0.63(h/D) + 0.052(h/D)^5)$. The determination of the characteristics equation requires four vertical-bending-related, four lateral-bending-related and two torsional-related boundary conditions. The ten boundary conditions with considering interaction are

$$W(0,t) = 0 \tag{4.a}$$

$$\frac{\partial W(0,t)}{\partial X} = 0 \tag{4.b}$$

$$EI_y \frac{\partial^2 W(L,t)}{\partial X^2} = -K_l H^2 \frac{\partial W(L,t)}{\partial X} \tag{4.c}$$

$$EI_y \frac{\partial^3 W(L,t)}{\partial X^3} = K_n W(L,t) \tag{4.d}$$

$$V(0,t) = 0 \tag{4.e}$$

$$\frac{\partial V(0,t)}{\partial X} = 0 \tag{4.f}$$

$$EI_z \frac{\partial^2 V(L,t)}{\partial X^2} = 0 \tag{4.g}$$

$$EI_z \frac{\partial^3 V(L,t)}{\partial X^3} = K_l (H\phi(L,t) + V(L,t)) \tag{4.h}$$

$$\phi(0,t) = 0 \tag{4.i}$$

$$GJ \frac{\partial \phi(L,t)}{\partial X} = -K_l H (H\phi(L,t) + V(L,t)) \tag{4.j}$$

At the built-in end the deflections and the slopes of the beam must be zero. Thus, if the end $X = 0$ is assumed to be built-in, then the boundary conditions given by Eqs. (4.a), (4.e) and (4.b), (4.f) correspond to conditions of zero displacements and slopes, respectively. The boundary conditions given by Eq. (4.i) correspond to zero twist angle. At the free end, the moments and the shear forces of the beam must be zero. Thus, if the end $X = L$ is assumed to be free, then boundary conditions given by Eqs. (4.c), (4.d), (4.g), (4.h) and (4.j) correspond to the moments balanced and forces balanced between the end beam with the linear springs K_n, K_l and K_t. For harmonic vibrations the displacements and torsional rotation can be expressed in the form of

$$W(X,t) = w(X)e^{i\omega t} \qquad V(X,t) = v(X)e^{i\omega t} \qquad \phi(X,t) = \varphi(X)e^{i\omega t} \tag{5}$$

Where ω is the angular frequency of vibration, the dimensionless parameters are defined as

$$x = \frac{X}{L} \qquad w = \frac{W}{L} \qquad v = \frac{V}{L} \tag{6.a}$$

$$b = \frac{H}{L} \qquad p^2 = \frac{\rho I_p L^2 \omega^2}{GJ} \tag{6.b}$$

$$s = \frac{GJ}{EI_y} \qquad q = \frac{GJ}{EI_z} \qquad r = \frac{AL^2}{I_p} \tag{6.c}$$

$$\gamma^4 = srp^2 \qquad \alpha^4 = qrp^2 \tag{6.d}$$

$$\beta_l = \frac{K_l H^2 L}{GJ} \qquad \beta_n = \frac{K_n H^3}{EI_y} \tag{6.e}$$

Utilizing these dimensionless parameters and substituting Eq. (5) into Eqs. (1) to (4), the coupled equations and the associated boundary conditions can be simplified to the following dimensionless differential equations and boundary conditions

$$\frac{d^4 w(x)}{dx^4} - \gamma^4 w(x) = 0 \tag{7}$$

$$\frac{d^4 v(x)}{dx^4} - \alpha^4 v(x) = 0 \tag{8}$$

$$\frac{d^2 \varphi(x)}{dx^2} + p^2 \varphi(x) = 0 \tag{9}$$

$$w(0) = 0 \tag{10.a}$$

$$\frac{dw(0)}{dx} = 0 \tag{10.b}$$

$$\frac{d^2 w(L)}{dx^2} = -\beta_l s \frac{dw(L)}{dx} \tag{10.c}$$

$$\frac{d^3 w(L)}{dx^3} = \beta_n w(L) \tag{10.d}$$

$$v(0) = 0 \tag{10.e}$$

$$\frac{dv(0)}{dx} = 0 \tag{10.f}$$

$$\frac{d^2 v(L)}{dx^2} = 0 \tag{10.g}$$

$$\frac{d^3 v(L)}{dx^3} = \frac{\beta_l q}{b}\left(\varphi(L) + \frac{1}{b} v(L)\right) \tag{10.h}$$

$$\varphi(0) = 0 \tag{10.i}$$

$$\frac{d\varphi(L)}{dx} = -\beta_l\left(\varphi(L) + \frac{1}{b} v(L)\right) \tag{10.j}$$

2.2. Solution

The general solutions of Eqs. (7) to (9) can be expressed as

$$w(x) = A_1 \sin(\gamma x) + A_2 \cos(\gamma x) + A_3 \sinh(\gamma x) + A_4 \cosh(\gamma x) \tag{11}$$

$$v(x) = B_1 \sin(\alpha x) + B_2 \cos(\alpha x) + B_3 \sinh(\alpha x) + B_4 \cosh(\alpha x) \tag{12}$$

$$\varphi(x) = C_1 \sin(px) + C_2 \cos(px) \tag{13}$$

Where $A_1 ... A_4$, $B_1 ... B_4$ and C_1, C_2 are the constants to be determined from the boundary conditions. By substituting the Eqs. (11) to (13) into the boundary conditions, (10), a characteristic equation can be obtained to determine the resonance frequencies. This leads to the following characteristic equation

$$\begin{aligned} C(p,\beta_n,\beta_l) = \frac{1}{b^2}\Big[&\alpha^3\gamma^2\Big(\big(\beta_n\beta_l s+\gamma^4\big)\cosh^2(\gamma L)+\big(2\gamma\big(\beta_n+\beta_l s\gamma^2\big)\sin(\gamma L)-2\big(\beta_n\beta_l s+\gamma^4\big)\\ &\cos(\gamma L)\big)\cosh(\gamma L)+\big(\beta_n\beta_l s+\gamma^4\big)\cos^2(\gamma L)-2\gamma\big(\beta_n-\beta_l s\gamma^2\big)\sinh(\gamma L)\cos(\gamma L)+\\ &\big(\sin^2(\gamma L)-\sinh^2(\gamma L)\big)\big(\beta_n\beta_l s+\gamma^4\big)\Big)\Big(\big(\alpha^3 b^2\cosh^2(\alpha L)+2\big(\alpha^3 b^2\cos(\alpha L)+\beta_l q\sin(\alpha L)\big)\\ &\cosh(\alpha L)+\alpha^3 b^2\cos^2(\alpha L)-2\beta_l q\cos(\alpha L)\sinh(\alpha L)+\alpha^3 b^2 p\cos(pL)\\ &\big(\sin^2(\alpha L)-\sinh^2(\alpha L)\big)\big)+\alpha^3 b^2\beta_l\sin(pL)\big(2\big(1+\cosh(\alpha L)\cos(\alpha L)\big)\big)\Big] \end{aligned} \tag{14}$$

The roots of Eq. (14) are the eigenvalue or natural frequencies of the system. The resonant frequency based on the dimensionless parameter $p^2 = \rho I_p L^2 \omega^2 / GJ$ in Eq. (6.b) is obtained, and is given as

$$f = \frac{p}{2\pi}\sqrt{\frac{GJ}{\rho I_p L^2}} \tag{15}$$

The sensitivity of the probe can be calculated from the frequency, which can be measured. The sensitivity is defined as the change in the vibration frequency of a mode with respect to the change in normal or lateral contact stiffness [7,8]. Once differentiation of Eq. (14) with respect to β_n implies that

$$\frac{dp}{d\beta_n} = -\frac{\partial C/\partial\beta_n}{\partial C/\partial p} \tag{16}$$

The relationship between frequency f and normal contact stiffness, β_n, can be expressed as

$$\frac{\partial f}{\partial\beta_n} = \frac{\partial f}{\partial p}\frac{\partial p}{\partial\beta_n} = \frac{1}{2\pi}\sqrt{\frac{GJ}{\rho I_p L^2}}\frac{\partial p}{\partial\beta_n} \tag{17}$$

The dimensionless form of the sensitivity due to normal contact stiffness is given by

$$S_n = \frac{\partial f/\partial\beta_n}{(1/2\pi)\sqrt{GJ/\rho I_p L^2}} = \frac{\partial p}{\partial\beta_n} \tag{18}$$

Thus,

$$S_n = -\Big[\big(\beta_l s\cosh^2(\gamma L) + 2\big(\gamma\sin(\gamma L) - \beta_l s\cos(\gamma L)\big)\cosh(\gamma L) + \beta_l s\cos^2(\gamma L) - 2\gamma\sinh(\gamma L)\cos(\gamma L) + \beta_l s\big(\sin^2(\gamma L) - \sinh^2(\gamma L)\big)\big)\big(p\cos(pL)\big(\alpha^3 b^2\cosh^2(\alpha L) + 2\big(\alpha^3 b^2\cos(\alpha L) + \beta_l q\sin(\alpha L)\big)\cosh(\alpha L) + \alpha^3 b^2\cos^2(\alpha L) - 2\beta_l q\cos(\alpha L)\sinh(\alpha L) + \alpha^3 b^2\big(\sin^2(\alpha L) - \sinh^2(\alpha L)\big)\big) + \beta_l\alpha^3 b^2\sin(pL)\big(2\big(1+\cos(\alpha L)\cosh(\alpha L)\big)\big)\big)\Big]/\Big[\big(\big(\beta_n\beta_l s + \gamma^4\big)\cosh^2(\gamma L) + \big(2\big(\gamma^4 - \beta_n\beta_l s\big)\cos(\gamma L) + 2\gamma\big(\beta_l s\gamma^2 + \beta_n\big)\sin(\gamma L)\big)\cosh(\gamma L) + \big(\beta_n\beta_l s + \gamma^4\big)\cos^2(\gamma L) - 2\gamma\big(\beta_n - \beta_l s\gamma^2\big)\cos(\gamma L)\sinh(\gamma L) + \big(\gamma^4 + \beta_n\beta_l s\big)\big(\sin^2(\gamma L) - \sinh^2(\gamma L)\big)\big)\big(\big(\alpha^3 b^2\big(1+\beta_l L\big)\cosh^2(\alpha L) + \big(2\alpha^3 b^2\big(1+\beta_l L\big)\cos(\alpha L) + 2\beta_l q\sin(\alpha L)\big)\cosh(\alpha L) + \alpha^3 b^2\big(1+\beta_l L\big)\cos^2(\alpha L) - 2\beta_l q\cos(\alpha L)\sinh(\alpha L) + \alpha^3 b^2\big(\sin^2(\alpha L) - \sinh^2(\alpha L)\big)\big)\cos(pL) - \big(\alpha^3 b^2\cosh^2(\alpha L) + 2\big(\alpha^3 b^2\cos(\alpha L)\beta_l q\sin(\alpha L)\big)\cosh(\alpha L) + \alpha^3 b^2\cos^2(\alpha L) - 2\beta_l q\cos(\alpha L)\sinh(\alpha L) + \alpha^3 b^2\big(\sin^2(\alpha L) - \sinh^2(\alpha L)\big)\big)pL\sin(pL)\big)\Big] \tag{19}$$

The sensitivity due to lateral contact stiffness is derived in the same way as the sensitivity due to normal contact stiffness. Consequently, differentiation of Eq. (14) with respect to β_l implies that

$$\frac{dp}{d\beta_l} = -\frac{\partial C/\partial\beta_l}{\partial C/\partial p} \tag{20}$$

Therefore, the sensitivity due to lateral contact stiffness is given by

$$S_l = -\Big[\big(\big(\alpha^3\big(2pq\big(\sin(\alpha L)\cosh(\alpha L) - \cos(\alpha L)\sinh(\alpha L)\big)\cos(pL) + 2\alpha^3\gamma^2 b^2\sin(pL)\big(1+\cos(\alpha L)\cosh(\alpha L)\big)\big)\big(\big(\beta_n\beta_l s + \gamma^4\big)\cosh^2(\gamma L) + \big(2\big(\gamma^4 - \beta_n\beta_l s\big)\cos(\gamma L) + 2\gamma\big(\beta_n + \beta_l s\gamma^2\big)\sin(\gamma L)\big)\cosh(\gamma L) + \big(\beta_n\beta_l s + \gamma^4\big)\cos^2(\gamma L) - 2\gamma\big(\beta_n - \beta_l s\gamma^2\big)\sinh(\gamma L)\cos(\gamma L) + \alpha^3 b^2\cos(\alpha L)\big)\cosh(\alpha L) + \alpha^3 b^2\cos^2(\alpha L) - 2\beta_l q\cos(\alpha L)\sinh(\alpha L) + \alpha^3 b^2\big(\sin^2(\alpha L) - \sinh^2(\alpha L)\big)\big)\cos(pL) + 2\alpha^3 b^2\beta_l\sin(pL)\big(1+\cos(\alpha L)\cosh(\alpha L)\big)\big)\gamma^2\big(\beta_n s\cosh^2(\gamma L) + 2\big(s\gamma^3\sin(\gamma L) - \beta_n s\cos(\gamma L)\big)\cosh(\gamma L) + \beta_n s\cos^2(\gamma L) + 2s\gamma^3\cos(\gamma L)\sinh(\gamma L) + \beta_n s\big(\sin^2(\gamma L) - \sinh^2(\gamma L)\big)\big)\big)\Big]/\Big[\alpha^3\big(\big(\alpha^3 b^2\cosh^2(\alpha L) + 2\big(\beta_l q\sin(\alpha L) + \alpha^3 b^2\cos(\alpha L)\big)\cosh(\alpha L) + \alpha^3 b^2\cos^2(\alpha L) - 2\beta_l q\cos(\alpha L)\sinh(\alpha L) + \alpha^3 b^2\big(\sin^2(\alpha L) - \sinh^2(\alpha L)\big)\big)L\sin(pL) + \alpha^3 b^2\beta_l L\cos(pL)\big(2\big(1+\cos(\alpha L)\cosh(\alpha L)\big)\big)\big)\gamma^2\big(\big(\beta_n\beta_l s + \gamma^4\big)\cosh^2(\gamma L) + \big(2\big(\gamma^4 - \beta_n\beta_l s\big)\cos(\gamma L) + 2\gamma\sin(\gamma L)\big(\beta_n + \beta_l s\gamma^2\big)\big)\big)\Big] \tag{21}$$

From the above equations, the sensitivities due to normal and lateral contact stiffness as function of dimensionless parameters for each mode can be calculated.

3. Numerical Results and discussions

In this section, based on the presented analytical method, the frequency analysis and modal sensitivities of an AFM cantilever are focused. Numerical results are presented to reveal the influence of the normal and lateral contact stiffness and tip length on the coupled frequencies and modal sensitivities of the AFM cantilever. To validate the solution procedure, for the case of $\beta_l = \alpha = p = 0$ and $\gamma L = \gamma$ the characteristics equation (14) can be simplified as

$$C(\gamma, \beta_n) = \gamma^3\big(\cos\gamma\cosh\gamma + 1\big) - \beta_n\big(\sinh\gamma\cos\gamma - \sin\gamma\cosh\gamma\big) \tag{22}$$

The above frequency equation is the same as the form obtained by Turner and Wiehn [5]. While for the case of $\beta_n = \gamma = 0$, $\alpha L = \alpha$ and $pL = p$ the characteristic equation (14) can be reduced to

$$C(p,\beta_l)=(p\cos p+\beta_l \sin p)(1+\cos\alpha\cosh\alpha)+\frac{1}{b^2\alpha^3}\beta_l pq\cos p(\cosh\alpha\sin\alpha-\sinh\alpha\cos\alpha) \tag{23}$$

As can be seen, this is the same as the frequency equation obtained by Lee and Chang [11].

The resonant frequency and modal sensitivities were expressed as functions of geometrical and mechanical properties of probe and contact stiffnesses. The values of the geometrical and mechanical properties of this case-study probe are considered as $E=150$ GPa, $G=64$ GPa, $\rho=2300$ kg/m^3, $L=200$ μm, $D=40$ μm, $h=5$ μm, $H=15$ μm [11]. The lateral contact stiffness can be assumed as $K_l=0.9K_n$ [14]. The energy dissipation due to the tip–sample interaction is neglected. Once the normal and lateral contact stiffnesses are given, the natural frequencies and modal sensitivities of the tip–cantilever system under linear interactions tip–sample are obtained by solving the equations (14), (19) and (21). Each mode has a different resonant frequency and sensitivity to variations in contact stiffnesses. In the forthcoming figures, the modal sensitivities and resonant frequency of the first five vibration modes and the variations in the sensitivities and natural frequency of first mode at various tip lengths of the system will be shown. The resonant frequency of the first five vibration modes of the cantilever as a function of dimensionless normal and lateral contact stiffnesses, β_n and β_l are illustrated in Fig.2. and Fig.3, respectively. It can be observed that as β_n and β_l increase, the resonant frequency commences from a constant value at low values of normal and lateral contact stiffnesses then increases until it finally reaches another constant value at very high values of normal and lateral contact stiffnesses.

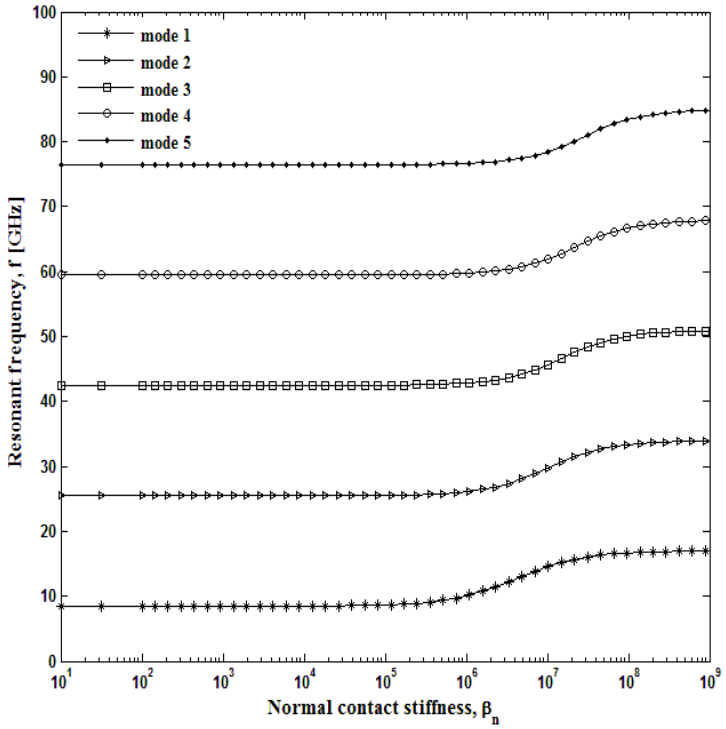

Fig. 2. The cantilever's first five resonant frequencies as a function of normal contact stiffness, β_n, for an AFM cantilever.

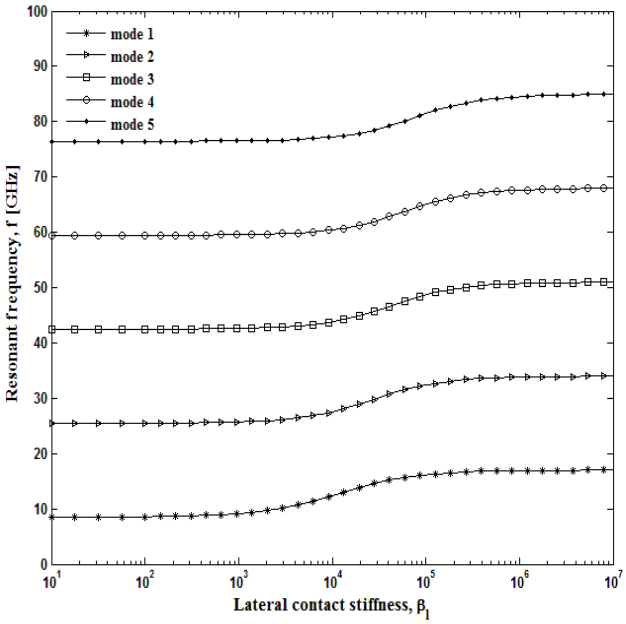

Fig. 3. The cantilever's first five resonant frequencies as a function of lateral contact stiffness, β_l , for an AFM cantilever.

The modal sensitivities of the first five vibration modes as a function of dimensionless normal and lateral contact stiffnesses, β_n and β_l are shown in Fig. 4 and Fig.5, respectively. It can be observed that as β_n and β_l increase, the modal sensitivities of all the vibration modes decreased. Moreover, for low normal and lateral contact stiffnesses, the low-order modes are more sensitive than high-order modes and the first mode is the most sensitive. Whereas the normal and lateral contact stiffnesses become larger, it can be noted that high-order modes become more sensitive. Comparing Fig.2 with Fig. 3, it can be seen that in comparison with the values of normal contact stiffness, frequency shift, due to the tip–sample interaction, occurs in lower values of lateral contact stiffness. Comparing Fig.4 with Fig. 5, it can be seen that the resonant frequencies are more sensitive to the variation of lateral contact stiffness with respect to the variation of normal contact stiffness.

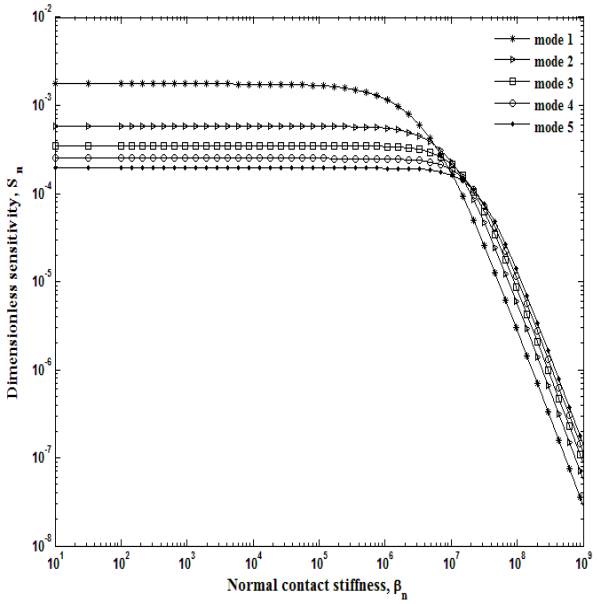

Fig. 4. Variation of sensitivity due to normal contact stiffness, S_n , as a function of β_n for an AFM cantilever for the first five modes.

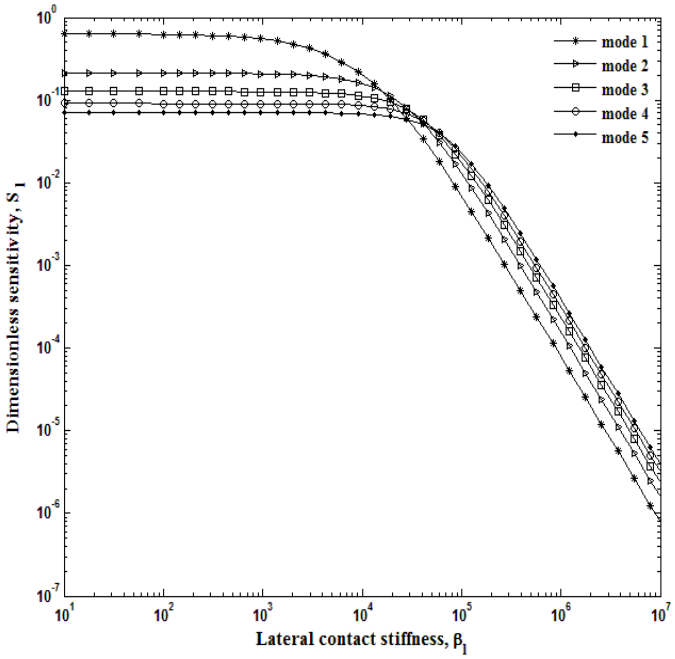

Fig. 5. Variation of sensitivity due to lateral contact stiffness, S_l, as a function of β_l for an AFM cantilever for the first five modes.

The tip length, H, can change sensitivity and the resonance frequency by producing a force and moment at the free end of the cantilever. Therefore, it is of interest to learn how the tip length affects modal sensitivities and resonant frequency of first mode. The resonant frequency of first mode of cantilever as a function of the normal contact stiffness, β_n, and the cantilever to tip lengths ratio, H/L, is shown in Fig. 6. This figure shows that increasing the tip length leads to increasing the resonance frequency when the normal contact stiffness, β_n, becomes large. The resonant frequency and dimensionless sensitivity of first mode of cantilever as functions of the lateral contact stiffness, β_l, and the cantilever to tip lengths ratio, H/L, are shown in Fig. 7 and Fig. 9, respectively. This figures show that for various lateral contact stiffness, β_l, increasing the cantilever to tip lengths ratio has little effects on the dimensionless sensitivity and resonance frequency. Dimensionless sensitivity of first mode of cantilever as a function of the normal contact stiffness, β_n, and the cantilever to tip lengths ratio, H/L, is depicted in Fig. 8. From this figure, it can be seen that at low and intermediate normal contact stiffnesses with the increase of the cantilever to tip lengths ratio, the dimensionless sensitivity increases. But at very high normal contact stiffness, β_n, increasing the tip length decreases the dimensionless sensitivity.

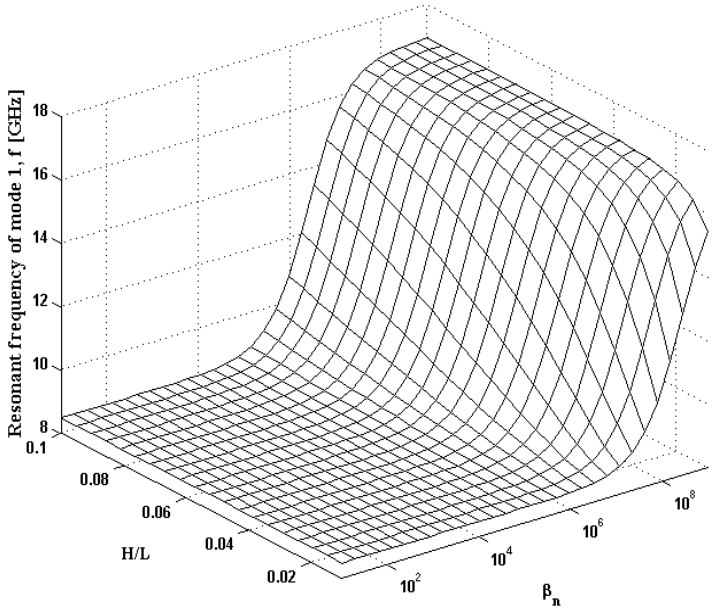

Fig. 6. Resonant frequency of first mode as a function of the normal contact stiffness, β_n, and the cantilever to tip lengths ratio, H/L.

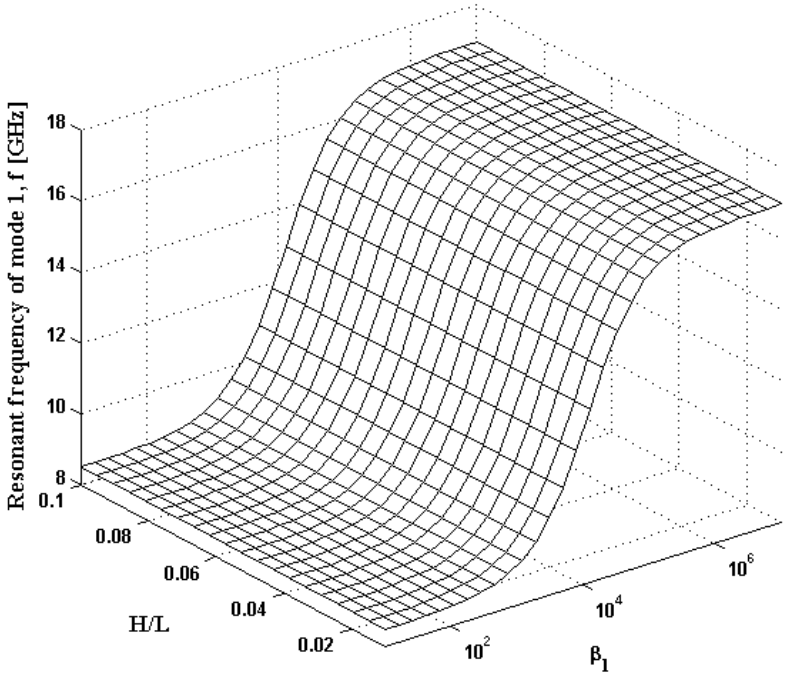

Fig. 7. Resonant frequency of first mode as a function of the lateral contact stiffness, β_l, and the cantilever to tip lengths ratio, H/L.

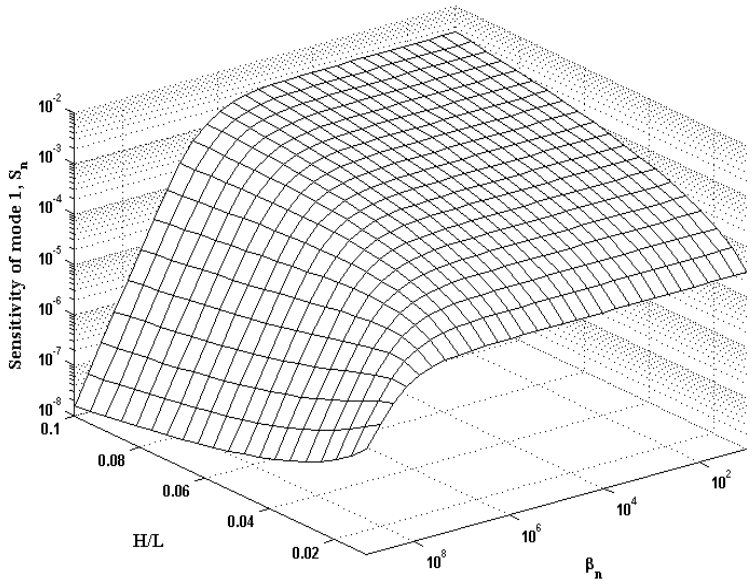

Fig. 8. Vibration sensitivity due to normal contact stiffness, S_n, of first mode as a function of β_n and the cantilever to tip lengths ratio, H/L.

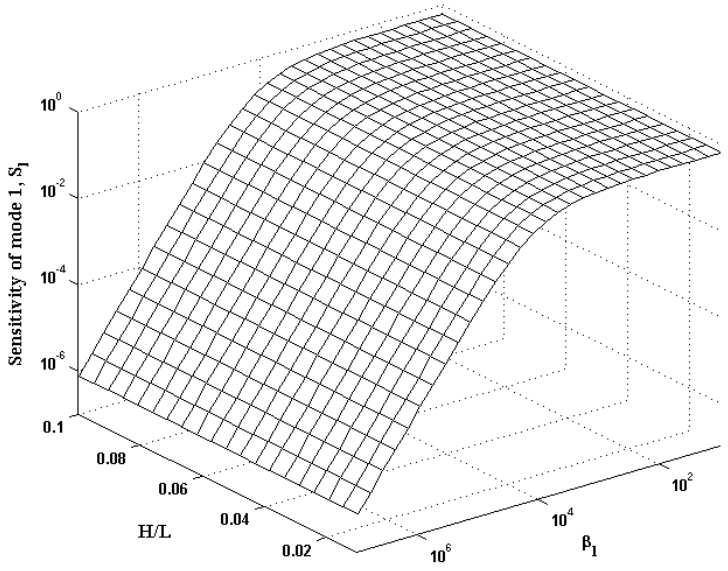

Fig. 9. Vibration sensitivity due to lateral contact stiffness, S_l, of first mode as a function of β_l and the cantilever to tip lengths ratio, H/L.

4. Conclusions

In this paper, the effects of tip length and normal and lateral contact stiffnesses on resonant frequency and the modal sensitivities of an AFM cantilever have been analyzed. According to the analysis, the results showed that with increasing normal and lateral contact stiffnesses, the resonant frequency increases until it finally reaches a constant value at very high values of contact stiffnesses. In addition, in comparison with the values of normal contact stiffness, frequency shift, due to the tip–sample interaction, occurs in lower values of lateral contact stiffness. It was also shown that in the low values of contact stiffnesses, the lower-order vibration modes are more sensitive than the higher-order modes. The situation is completely reversed in very high contact stiffnesses. Furthermore, the resonant frequencies are more sensitive to the variation of lateral contact stiffness with respect to the variation of normal contact stiffness. The results also indicate that for various lateral contact stiffness, increasing the cantilever to tip lengths ratio has little effects on the dimensionless sensitivity and resonance frequency of first mode.

Whereas increasing the cantilever to tip lengths ratio increases the resonance frequency when the normal contact stiffness, become greater. Besides, at low and intermediate normal contact stiffnesses with the increase of the cantilever to tip lengths ratio, the dimensionless sensitivity increases. But at very high normal contact stiffness, increasing the cantilever to tip lengths ratio leads to decreasing the dimensionless sensitivity.

References

[1] G. Binnig, C.F. Quat, C. Gerber, J. Phys. Rev. Lett. **56**, 930 (1986).
[2] B. Bhushan, Handbook of Nanotechnology, second ed., springer, Heidelberg (2005).
[3] Y. Song, B. Bhushan, J. Phys.: Condens. Matter. **20**, 225012 (2008).
[4] Y. Song, B. Bhushan, J. Ultramicroscopy. **106**, 847 (2006).
[5] Y. Song, B. Bhushan, J. Appl. Phys. **99**, 094911 (2006).
[6] Y. Song, B. Bhushan, J. Microsyst. Technol. **12**, 219 (2006).
[7] J.A. Turner, J.S. Wiehn, J. Nanotechnology. **12**. 322 (2001).
[8] W.J. Chang, Sensitivity of vibration modes of atomic force microscope cantilevers in continuous surface contact, J. Nanotechnology. **13**(2002) 510–514.
[9] W.J. Chang, T.H. Fang, H.M. Chou, J. Phys. Lett. A **312,** 158 (2003).
[10] J.C. Hsu, H.L. Lee, W.J. Chang, J. Nanotechnology. **18**, 285503 (2007).
[11] H.L. Lee, W.J. Chang, J. Ultramicroscopy. **108**, 707 (2008).
[12] M.H. Kahrobaiyan, M.T.Ahmadian, P.Haghighi, A.Haghighi, Int. J. Mech. Sci. **52**, 1357 (2010).
[13] D.J. Gorman, Free Vibration Analysis of Beams and Shafts, Wiley, New York (1975).
[14] O.B. Wright, N. Nishiguchi, J. Appl. Phys. Lett. **71**, 626 (1997).